Frustrated magnetism from local moments in FeSe

Harrison Ruiz,[1,2] Yao Wang,[2,3,4] Brian Moritz,[2,5] Andreas Baum,[6,7] Rudi Hackl,[6] and Thomas P. Devereaux[2]

[1]*Department of Physics, Stanford University, Stanford, California 94305, USA*

[2]*Stanford Institute for Materials and Energy Sciences, SLAC National Accelerator Laboratory and Stanford University, Menlo Park, California 94025, USA*

[3]*Department of Applied Physics, Stanford University, Stanford, California 94305, USA*

[4]*Department of Physics, Harvard University, Cambridge, Massachusetts 02138, USA*

[5]*Department of Physics and Astrophysics, University of North Dakota, Grand Forks, North Dakota 58202, USA*

[6]*Walther Meissner Institut, Bayerische Akademie der Wissenschaften, 85748 Garching, Germany*

[7]*Fakultät für Physik E23, Technische Universität München, 85748 Garching, Germany*

We investigate properties of a spin-1 Heisenberg model with extended and biquadratic interactions, which captures crucial aspects of the low energy physics in FeSe. While we show that the model exhibits a rich phase diagram with four different magnetic ordering tendencies, we identify a parameter regime with strong competition between Néel, staggered dimer, and stripelike magnetic fluctuations, accounting for the physical properties of FeSe. We evaluate the spin and Raman responses using exact diagonalization. Through comparison with experiments we find enhanced magnetic frustration between Néel and collinear stripe ordering tendencies, which increases with increasing temperature. The explanation of these spectral behaviors with this frustrated spin model supports the idea of local spin interactions in FeSe.

I. INTRODUCTION

Magnetic excitations are believed to play a significant role in the high-T_c copper and iron-based superconductors [1,2]. Among the latter, FeSe has gained attention recently, in part because of the discovery of a superconducting phase above 100 K [3] for monolayers grown on appropriate substrates. Bulk FeSe exhibits a superconducting transition temperature T_c of 9 K, which rises dramatically under pressure [4,5]; in contrast, a single-layer FeSe film deposited on SrTiO$_3$ substrate exhibits a T_c increased by an order of magnitude [6–9].

Like other iron chalcogenides, FeSe consists of alternating iron and chalcogenide planes, with van der Waals bonds holding together quasi-two-dimensional (2D) layers in the bulk [10,11]. When cooled across a characteristic temperature $T_S \sim 90$ K, FeSe undergoes a nematic transition that breaks C_4 crystal rotational symmetry in the iron plane with a tetragonal to orthorhombic structural transition [12,13]. While the iron pnictides display a collinear striped spin-density-wave (SDW) phase immediately following a similar structural transition [14–16], and other iron chalcogenides possess magnetic orders [17,18], no long-range magnetic order has been observed for FeSe [19].

Considering the critical role that spin fluctuations may play in the unconventional, iron-based superconductors [2,11,20], understanding the magnetic properties of iron chalcogenides, in particular FeSe, is helpful in identifying the nature of the pairing mechanism. To that end, experimental evidence from neutron scattering for magnetic frustration [19] and competing magnetic ordering tendencies found in mean-field theoretical solutions of spin models [21] paint a picture of finely balanced interactions among various magnetically ordered phases.

Experimental and theoretical evidence suggests that despite the fact that FeSe is a metal with itinerant electrons, the low energy physics in FeSe can be described well in terms of localized electrons, owing to strong electronic correlations [22–24], with a fluctuating magnetic moment of $\langle m^2 \rangle \sim 5 \, \mu_B^2$ per Fe atom [19] corresponding to $S = 1$.

A mean-field phase diagram for this type of localized electron model shows four dominant magnetic phases: Néel order $[(\pi, \pi)]$, a collinear striped phase $[(\pi, 0)$ or $(0, \pi)]$, a staggered dimer phase $[(\pi, \pi/2)$ and equivalent], and a double stripe phase $[(\pi/2, \pi/2)$ and equivalent] [21]. Previous experiments and first-principles studies have measured spin correlations consisting of multiple wave vectors, demonstrating a magnetic frustration lacking long-range order [19,24]. This motivates the use of a spin-1 Heisenberg model with long-range spin interactions in a regime with magnetic frustration [21,25]. Two regions of the phase diagram were previously identified as appropriate for FeSe: a parameter regime with competition between the Néel and collinear striped orders, and one between the staggered dimer and collinear striped orders.

II. MODEL AND METHODS

Here we study the physics of a spin-1 Heisenberg model on a two-dimensional, 16-site cluster using exact diagonalization. Through benchmarking with mean-field theory and two different experiments, our study sets the stage for investigating the nature of FeSe within the spin model. For parameters tuned to a frustrated region among the Néel order, staggered dimer, and collinear striped phases we evaluate the temperature dependence of the dynamical spin structure factor $S(\mathbf{q}, \omega)$ and the Raman scattering cross section. Consistent

with neutron scattering [19], we find intense fluctuations of the collinear stripe order at low temperatures that give way to enhanced fluctuations at the Néel order wave vector for higher temperatures. Raman scattering [26] suggests a dominant spin character for a persistent peak in the B_{1g} symmetry close to 60 meV, which softens slightly at higher temperatures.

Due to strong electron correlations and the fluctuating magnetic moment, which neutron experiments have found to correspond well with a $S = 1$ system [19], the spin-1 J_1-J_2-J_3-K Heisenberg model, and similar variants, have been used to study the magnetic properties of FeSe [21,25]. The Hamiltonian can be written as

$$\mathcal{H} = \sum_{\langle i,j \rangle} [J_1 \, \mathbf{S}_i \cdot \mathbf{S}_j + K (\mathbf{S}_i \cdot \mathbf{S}_j)^2]$$
$$+ \sum_{\langle\langle i,j \rangle\rangle} J_2 \, \mathbf{S}_i \cdot \mathbf{S}_j + \sum_{\langle\langle\langle i,j \rangle\rangle\rangle} J_3 \, \mathbf{S}_i \cdot \mathbf{S}_j, \qquad (1)$$

where $\mathbf{S}_i = (S_i^x, S_i^y, S_i^z)$ is a spin operator at site i, $J_\alpha (\alpha = 1, 2, 3)$ are the nearest, next-nearest, and next-next-nearest-neighbor exchange interactions, and K is the nearest-neighbor biquadratic interaction. The nearest-neighbor exchange term J_1 favors a Néel state, while the longer-range exchange terms (J_2 and J_3) frustrate it. A large J_2 or J_3 can overwhelm J_1 and drives the staggered dimer or double stripe phase [21]. In addition, the biquadratic term K modulates fluctuations depending on the sign: a negative K suppresses quantum fluctuations towards an Ising-like model [21], while a positive K enhances quantum fluctuations [27] and has been found to favor a semiordered semiclassical ground state, containing some correlations between neighboring sites in an otherwise disordered system [28]. In this work we adopt a small positive K to enhance quantum fluctuations.

We study the model on a 4×4 cluster with periodic boundary conditions. This 16-site system provides access to all the relevant momenta, while remaining computationally tractable for the temperature range of interest. While determining the ground state for such a problem is not computationally challenging, a study of the temperature dependence requires an accurate evaluation of the excited states to cover an energy spectrum in excess of the thermal energy scale set by the temperature T. We adopt the parallel Arnoldi method [29] to determine the eigenstates and energies, and use the continued fraction expansion [30] to calculate the finite-temperature dynamical structure factor and Raman response function.

A crucial task of this work is determining a physical set of model parameters, within the J_1-J_2-J_3-K Heisenberg model, that accounts for the low-energy properties of FeSe. To examine its dominant magnetic fluctuations and ordering instability as a function of these parameters, we first evaluate the static spin correlation function

$$S(\mathbf{q}) = \frac{1}{N} \sum_l e^{i\mathbf{q}\cdot\mathbf{r}_l} \sum_i \langle \mathbf{S}_{\mathbf{r}_i+\mathbf{r}_l} \cdot \mathbf{S}_{\mathbf{r}_i} \rangle, \qquad (2)$$

where $\mathbf{r}_l$ represents the coordinate of site l on the cluster and the expectation value is taken with respect to the ground state at zero temperature. To fairly parametrize the relative strength of fluctuations with different characteristic wave vectors, we normalize the relative intensity of the dominant and largest subdominant correlation functions. Thus, the relative strength
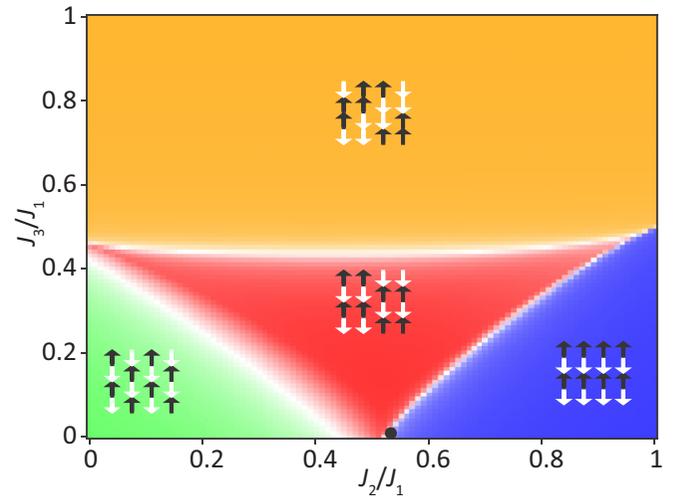
FIG. 1. Zero temperature "phase diagram" for the J_1-J_2-J_3-K spin-1 Heisenberg model with $K = 0.1 J_1$. The four different colors represent regions in parameter space dominated by fluctuations of the spin arrangement depicted in each cartoon, where green is Néel, red is staggered dimer, blue is collinear stripe, and orange is double stripe. The color intensity denotes the relative strength I, as defined in Eq. (3). The black circle ($J_2 = 0.528 J_1$, $J_3 = 0$) denotes parameters for which we calculate the dynamical spin structure factor and Raman susceptibility as a function of temperature.

of fluctuations is projected onto the range [0,1) by

$$I = 1 - \frac{d_{\mathbf{q}_{\text{sub}}} S(\mathbf{q}_{\text{sub}})}{d_{\mathbf{q}_{\text{dom}}} S(\mathbf{q}_{\text{dom}})}, \qquad (3)$$

where $d_{\mathbf{q}}$ is the geometric degeneracy for each equivalent momentum point on the 4×4 cluster and $\mathbf{q}_{\text{dom/sub}}$ denotes the value of $\mathbf{q}$ for which $d_{\mathbf{q}}S(\mathbf{q})$ is largest (dominant)/second largest (subdominant). Figure 1 shows the resulting phase diagram, which displays the order with the dominant correlation not the true long-range order of the system, obtained in this manner for the J_1-J_2-J_3-K model. Clearly, in contrast to the Néel order state (green) in the canonical Heisenberg model, the next-nearest-neighbor exchange J_2 favors a collinear striped state (blue) while the longer-range J_3 stabilizes a double stripe state (orange) above some critical couplings. In the middle of these three states, the combined impact of exchange interactions induces a staggered dimer region (red). Near the boundaries large fluctuations due to frustration suppress the states (white regions).

Given the various instabilities of the J_1-J_2-J_3-K model, can one find a parameter regime appropriate for FeSe? Previously, Wang *et al.* adopted a J_1-J_2 model near the quantum paramagnetic phase around $J_2 \sim 0.5 J_1$ [25] and Wang *et al.* suggested a point in the staggered dimer region near the boundary with collinear striped order (for negative K) [19]. Both involve competition between collinear striped order and some other state. This would be consistent with recent neutron scattering data, showing both collinear striped and, slightly weaker, Néel order fluctuations at low temperatures, with spectral weight transfer between them upon changing the temperature. Such an experimental observation suggests that the low-energy

magnetic properties of FeSe can be described by a parameter set inside the collinear stripe region close to its boundary.

III. SPECTRAL RESULTS

In addition to neutron scattering, the Raman response provides another clue about a proper parameter regime for FeSe as it captures the two-magnon excitations. As a collective mode, the two-magnon excitations depend sensitively on the form and strength of magnetic interactions [31]. At low energy, the experimental Raman response in B_{1g} symmetry consists of two dominant contributions which can be separated in the temperature range around T_S [26]. The peak in the range below 200 cm^{-1} was interpreted previously in terms of charge nematic fluctuations [32]. We return to this point briefly later. Here we focus on the broad peak centered at 500 cm^{-1} which softens slightly and loses weight with increasing temperature [26]. We argue that this part of the Raman response originates from spin excitations and will elaborate now on the theoretical details.

In the Fleury-Loudon formalism [31], the Raman scattering operator is written as $\hat{O} = \sum_{i,j} J_{ij}(\hat{\mathbf{e}}_{\text{in}} \cdot \hat{\mathbf{d}}_{ij})(\hat{\mathbf{e}}_{\text{out}} \cdot \hat{\mathbf{d}}_{ij}) \mathbf{S}_i \cdot \mathbf{S}_j$ [33], where J_{ij} are exchange coupling strengths in the spin Hamiltonian, $\hat{\mathbf{d}}_{ij}$ represent unit vectors connecting sites i and j, and $\hat{\mathbf{e}}_{\text{in/out}}$ are the polarization vectors for the incoming/outgoing photons, respectively. The light polarizations that encode the Raman symmetry channels are

$$\hat{\mathbf{e}}_{\text{in}} = \frac{1}{\sqrt{2}}(\hat{x} + \hat{y}), \quad \hat{\mathbf{e}}_{\text{out}} = \frac{1}{\sqrt{2}}(\hat{x} + \hat{y}) \quad \text{for } A'_{1g},$$

$$\hat{\mathbf{e}}_{\text{in}} = \hat{x}, \quad \hat{\mathbf{e}}_{\text{out}} = \hat{y} \quad \text{for } B_{2g}, \tag{4}$$

$$\hat{\mathbf{e}}_{\text{in}} = \frac{1}{\sqrt{2}}(\hat{x} + \hat{y}), \quad \hat{\mathbf{e}}_{\text{out}} = \frac{1}{\sqrt{2}}(\hat{x} - \hat{y}) \quad \text{for } B_{1g},$$

where $A'_{1g} = A_{1g} \oplus B_{2g}$. In this work we mainly focus on the B_{1g} channel as it directly reveals the two-magnon excitation, while the A_{1g} and B_{2g} spectra serve as additional experimental comparison.

Using the Raman scattering operator $\hat{O}_\alpha$, we evaluate the temperature-dependent Raman response in different symmetry channels as

$$R_\alpha(\omega) = -\sum_n \frac{e^{-\beta E_n}}{\pi Z} \text{Im}\langle \psi_n | \hat{O}_\alpha^\dagger W^{-1} \hat{O}_\alpha | \psi_n \rangle, \tag{5}$$

where α denotes a particular symmetry channel, Z is the partition function, $W = \omega + E_n + i\epsilon - \mathcal{H}$, and $|\psi_n\rangle$ and E_n are the nth eigenstate and energy, with the sum taken over all eigenstates of the Hamiltonian in Fock space [30]. We use $\epsilon = 0.15J_1$ in the continued fraction step. To remove the elastic peak, it is convenient to calculate the Raman susceptibility $\chi''_\alpha(\omega) = R_\alpha(\omega) - R_\alpha(-\omega)$. Due to the computational challenges, we truncate the summation at an energy $E_0 + 2J_1$, while providing sufficient states for evaluating the temperature dependence of spectra up to $T = 0.25J_1$ (all states contributing a weight $e^{-\beta E_n} > e^{-5}$).

As shown in Fig. 2, the Raman susceptibility at zero temperature changes dramatically with J_2. In B_{1g} symmetry (middle panel) the two-magnon excitation starts around an energy of $7.5J_1$ for $J_2 = 0$, then softens uniformly approaching the
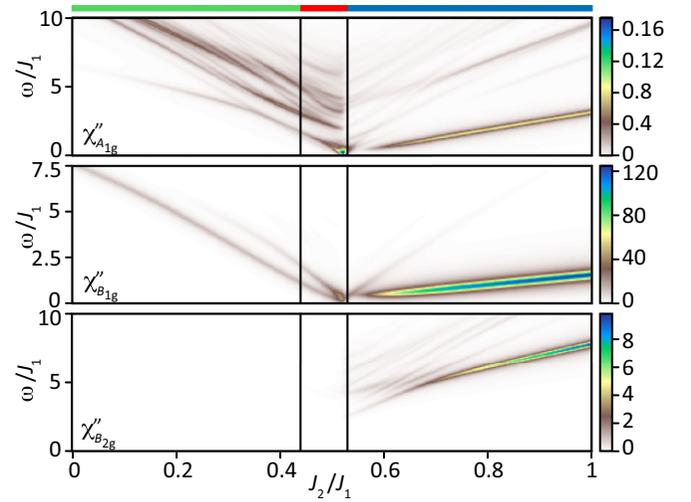
FIG. 2. Raman susceptibility $\chi''(\omega)$ at zero temperature as a function of J_2, with $J_3 = 0$ and $K = 0.1J_1$ for A_{1g} (top), B_{1g} (middle), and B_{2g} (bottom) symmetries. The two vertical black boundary lines and the top color bar sketch regions with distinct dominant correlations [Néel order (left), staggered dimer (middle), and collinear stripe (right), as in Fig. 1].

boundary between the staggered dimer and collinear striped phases. The energy for this two-magnon excitation can be estimated by counting the number of interactions that change sign with a double spin flip. Across the transition from Néel to staggered dimer, the transition is gradual as demonstrated by the wide white region in Fig. 1. In contrast, the transition across staggered dimer and collinear stripe order is more abrupt and leads to discontinuous changes in the Raman spectra. Taking a value of $J_1 = 123.1$ meV from first-principles calculations [21], it becomes clear that consistency between the experimental position of the peak at roughly 500 cm^{-1} and the theoretical two-magnon energy can only be obtained for $J_2/J_1 \sim 0.5$, near the boundary between the staggered dimer and collinear striped phases. This parameter range is also consistent with the general notion of highly frustrated magnetism in FeSe. We identify the best agreement in this region with $J_2 = 0.528J_1$, $J_3 = 0$, and $K = 0.1J_1$ (the black dot shown in Fig. 1). The significance of these parameters is presumably the positive biquadratic coupling K and the J_2 value that puts the system very close to the phase boundary in the immediate vicinity of the collinear stripe region. The exact numerical values of the parameters that describe FeSe are expected to change slightly in other finite size clusters and in the thermodynamic limit. As we show next, the finite temperature Raman and neutron scattering experiments compare favorably with simulations for these parameters.

Figure 3 displays the temperature dependence of the B_{1g} Raman susceptibility for the chosen parameters. We observe a single dominant peak. With increasing temperature, this peak softens slightly, before hardening again at higher temperature. The peak gradually loses intensity up to the highest simulated temperatures. In fact, thermal broadening occurs in all symmetries, while B_{1g} remains dominant. This dominant peak that softens with increasing temperature before hardening again agrees well with experiment [26], suggesting that a local
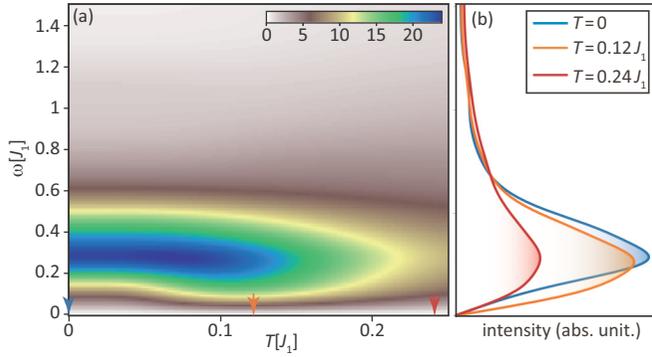
FIG. 3. (a) The imaginary part of the Raman susceptibility for B_{1g} symmetry as a function of temperature. (b) Cuts of Raman spectra at $T = 0$ (blue), $0.12J_1$ (orange), and $0.24J_1$ (red), indicated by the arrows.

spin model provides an adequate description of the dominant degrees of freedom in Raman scattering from FeSe in this energy range. We will see that the temperature dependence of this softening coincides with the temperature dependence of spectral weight transfer observed in $S(\mathbf{q} = (\pi, \pi), \omega)$, further reinforcing the connection between the peak in the Raman response and two magnon excitations.

The spectral range below the magnon excitations is dominated by critical fluctuations peaking at 50 cm^{-1} close to T_S [26,32]. The origin of these fluctuations is not obvious. While Massat *et al.* argue for orbital (charge) fluctuations [32] critical spin fluctuations cannot *a priori* be excluded in the ubiquitous presence of magnetism. Yet, our simulations in the spin channel do not support this interpretation. However, critical fluctuations cannot be captured by a simulation on a 4×4 cluster since they are characterized by a diverging correlation length for $T \to T_S$. The shoulder on the low-energy side of the magnon excitation may be a remainder of the fluctuations but further studies are necessary.

In A_{1g} symmetry [Fig. 4(a)], there is a single peak at slightly higher energy than the one found in the B_{1g} channel.
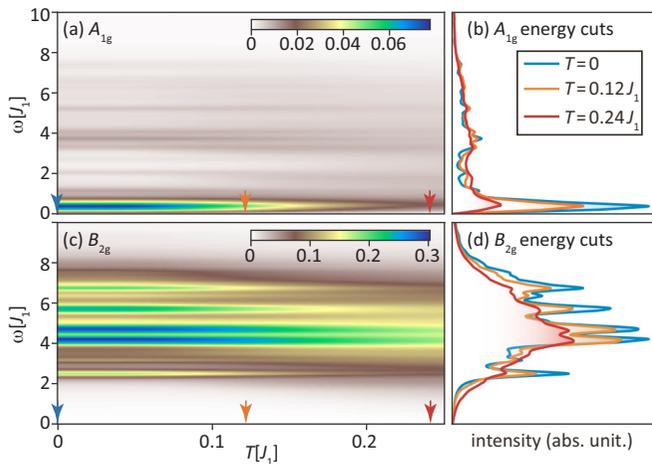
FIG. 4. The imaginary part of the Raman susceptibility for (a) A_{1g} and (c) B_{2g} symmetries at temperatures as indicated. (b) and (d) Cuts corresponding to A_{1g} and B_{2g} Raman spectra at three temperatures $T = 0$, $0.12J_1$, and $0.24J_1$.
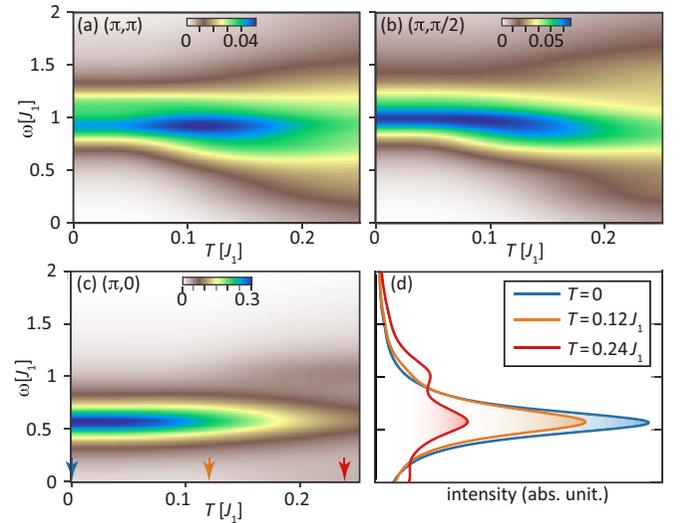
FIG. 5. (a)–(c) $S(\mathbf{q}, \omega)$ as a function of temperature for $\mathbf{q} = (\pi, \pi)$ (Néel), $\mathbf{q} = (\pi, \frac{\pi}{2})$ (staggered dimer), and $\mathbf{q} = (\pi, 0)$ (collinear stripe), respectively. More detailed temperature dependence can be seen for three temperature cuts of $(\pi, 0)$ in (d). As temperature increases, spectral weight shifts to lower energy at (π, π) and $(\pi, \frac{\pi}{2})$, and to higher energy at $(\pi, 0)$.

This peak decreases in intensity and hardens slightly with increasing temperature. In B_{2g} symmetry, shown in Fig. 4(b), we see several peaks spread out over the energy range of $2J_1$ to $8J_1$. The general trends for each of these symmetries, and in particular the dominant peak in B_{1g} symmetry, correspond well with recent Raman scattering data [26].

While we have seen that Raman scattering provides some information about magnetic excitations in the model, much more detailed information comes from the dynamical spin structure factor

$$S(\mathbf{q}, \omega) = -\sum_n \frac{e^{-\beta E_n}}{\pi Z} \operatorname{Im}\langle \psi_n | S^z_{-\mathbf{q}} W^{-1} S^z_{\mathbf{q}} | \psi_n \rangle, \qquad (6)$$

where $S^z_{\mathbf{q}} = \frac{1}{\sqrt{N}} \sum_l e^{i\mathbf{q} \cdot \mathbf{r}_l} S^z_l$. Figure 5 shows $S(\mathbf{q}, \omega)$ as a function of temperature for $\mathbf{q} = (\pi, 0)$, (π, π), and $(\pi, \frac{\pi}{2})$. At $T = 0$, the lowest-energy spin excitation occurs at $(\pi, 0)$, with significant fluctuations at slightly higher energy in $(\pi, \frac{\pi}{2})$ and (π, π), indicative of a frustrated magnetic system. With increasing temperature, the spin excitation at $(\pi, 0)$ hardens slightly and loses intensity, while it softens substantially at (π, π) and $(\pi, \frac{\pi}{2})$. This temperature dependence is reminiscent of the neutron scattering data [19], and the enhanced competition is consistent with the evolution of the B_{1g} Raman response in Fig. 3, further highlighting the role of magnetic frustration in FeSe.

IV. DISCUSSION

Interestingly, only a small region of parameter space with $K \sim 0.1J_1$ displays a temperature dependence consistent with the B_{1g} Raman and the spin response, at least in this 16-site cluster calculation (Raman response functions for other parameters shown in the Appendix B). The origin of this softening and its sensitivity to K is difficult to assess in a
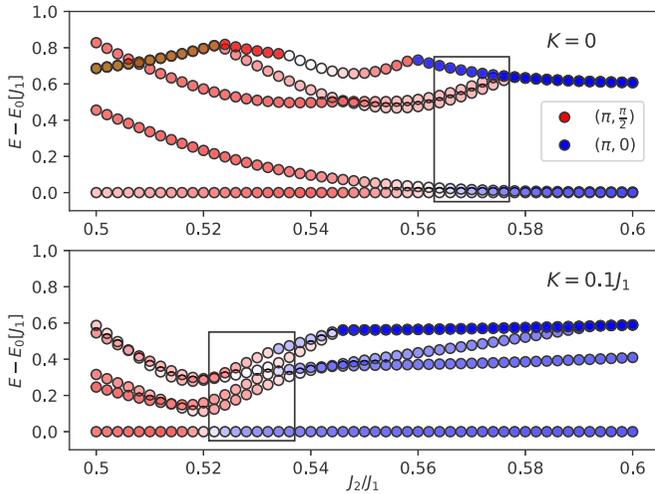
FIG. 6. Energy and magnetic fluctuations associated with the five lowest energy excited states for $K = 0$ (top) and $0.1J_1$ (bottom), as a function of J_2 for $J_3 = 0$. The black boxes enclose a range of J_2 where the ground state and possibly a nearly degenerate state of collinear striped order are followed by states characterized by a dominant staggered dimer phase. The color coding of each circle follows the same convention as Fig. 1.

simple spin-wave picture due to the many-body nature of this biquadratic term. Fortunately, with the full wave functions obtained by exact diagonalization, we can study the magnetic fluctuations and competition directly through eigenstates of the Hamiltonian. Figure 6 shows detailed information about the five lowest eigenstates as a function of J_2 for two different values of K. The color of each point represents the dominant magnetic character of the eigenstate, following the same convention as Fig. 1. Crossing the boundary to the collinear striped phase, there is a small region (highlighted by the black boxes) where the low-lying excited states possess a staggered dimer or mixed character. In this region, while both values of K result in similar ground states and zero-temperature Raman and neutron scattering spectra, only $K = 0.1J_1$ provides the ingredients for a temperature dependence consistent with

experiments, because of its much smaller excitation gap and larger density of excited states. These states are responsible for the softening of the B_{1g} peak, as well as the energy shift and weight transfer of the dynamical spin structure factor.

V. CONCLUSION

In summary, we present a systematic exact-diagonalization study of the magnetic fluctuations and spectra in a local spin J_1-J_2-J_3-K model. This model displays a rich phase diagram influenced by magnetic frustration. A comparison of the dynamical spin and Raman response to experimental results underscores that this model provides a consistent description of the magnetic properties of FeSe, lying at the boundary between the collinear stripe, Néel order, and staggered dimer phases. Through a detailed analysis of the eigenstates, we attribute the temperature evolution of the spectra to the competition between various finely balanced magnetic ground and excited states, and hence explain the crucial role of the biquadratic coupling. Our results suggest that magnetic frustration plays a dominant role in the low-energy physics of FeSe, which may additionally support the intrinsic connection between spin fluctuations and unconventional superconductivity. We find that local spins give an adequate description of these magnetic properties.
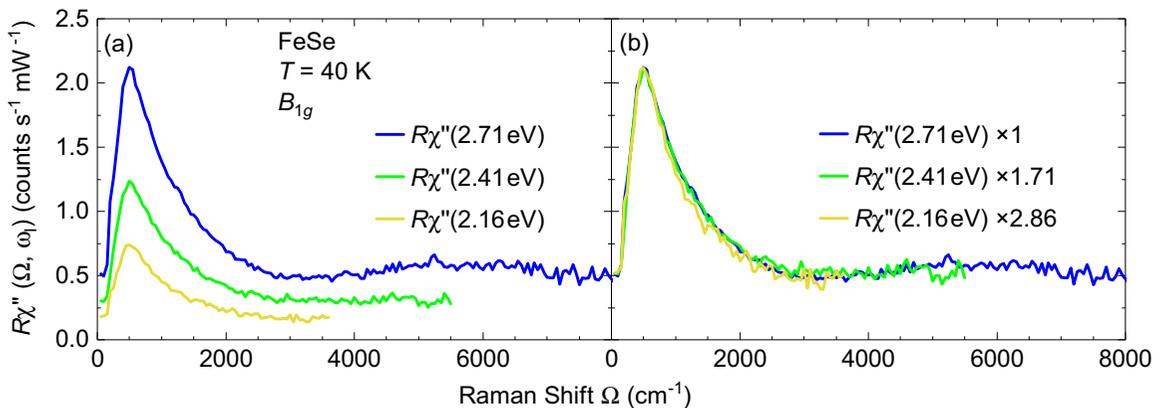
FIG. 7. B_{1g} Raman response $R\chi''(\Omega, \hbar\omega_I)$ of FeSe for three photon energies $\hbar\omega_I$ as indicated. All spectra are corrected for the instrumental response. (a) Raw data. At low energies the magnetic response is superimposed on the particle-hole continuum (see also Sec. 4 of the Supplemental Material in Ref. [26]). At high energies, $\Omega > 2000$ cm^{-1}, there is a substantial contribution from luminescence. (b) After appropriately multiplying the spectra measured with green and yellow photons with constant factors all spectra collapse on top of each other.
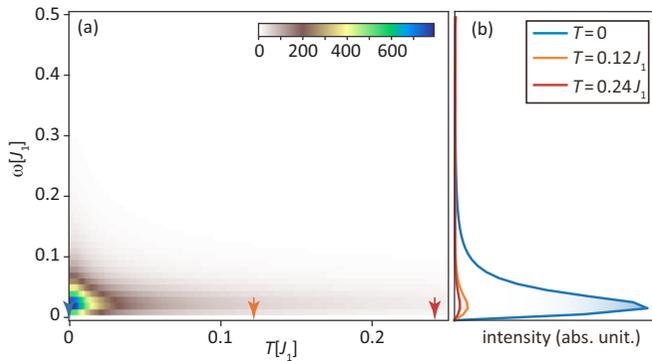
FIG. 8. The imaginary part of the Raman susceptibility for B_{1g} symmetry for $K = 0$, $J_2 = 0.57J_1$, and $J_3 = 0$. These parameters are found in the collinear stripe region near the transition to staggered dimer.

FIG. 10. The imaginary part of the Raman susceptibility for B_{1g} symmetry for $K = 0.2J_1$, $J_2 = 0.47J_1$, and $J_3 = 0$. These parameters are found in the collinear stripe region near the transition to staggered dimer.

APPENDIX A: LINE SHAPE OF THE B_{1g} RAMAN SPECTRA OF FeSe

The interaction of photons and spin excitations may be described by the Fleury-Loudon Hamiltonian O [31]. The Raman response is then determined as described in Eq. (5) of the main text. The Fleury-Loudon formalism is justified only in the nonresonant case. If the intermediate electronic states are eigenstates of the band structure not only the intensity but also the line shape may depend on the energy of the photons [34–36].

For justifying the applicability of the formalism we measured the B_{1g} Raman response of FeSe for three different excitation energies $\hbar\omega_I$, 2.16 eV (575 nm), 2.41 eV (514 nm), and 2.71 eV (458 nm) [λ_I (nm) = $1240/\hbar\omega_I$ (eV)]. The results are shown in Fig. 7. Figure 7(a) displays the raw data at 40 K after correcting for the spectral response of the system. All spectra peak at approximately 530 cm^{-1}, and the maxima are asymmetric having a much slower decay on the high-energy side than at low energies. The overall intensity increases by a factor of almost 3 if $\hbar\omega_I$ increases from 2.16 to 2.71 eV. Figure 7(b) shows that the line shape is independent of the excitation energy. All spectra collapse on top of each other

when multiplied appropriately. Thus the line shape does not depend on $\hbar\omega_I$. Consequently, the response derived via Eq. (5) of the main text is qualitatively correct. The experimental and theoretical results are compared in Figs. 3 and 5 of Ref. [26].

APPENDIX B: BIQUADRATIC COUPLING DEPENDENCE OF RAMAN SPECTRA

We have found the positive biquadratic coupling to be critical to the temperature dependence of the Raman susceptibility simulations agreeing well with experiment. Here we show nonzero temperature simulations for $K = 0$ and $K = 0.2J_1$. We have picked parameters immediately inside the collinear stripe region near the transition to staggered dimer along $J_3 = 0$, similar to the point highlighted in Fig. 1 of the main text.

Figure 8 shows the B_{1g} Raman susceptibility for $K = 0$. This was calculated in the same way as in the main text except that we used $\epsilon = 0.03J_1$ since the energy levels are more closely packed. The spectrum still consists of a dominant low energy peak but this peak does not soften as temperature is increased, a signature of Raman scattering in FeSe in B_{1g} symmetry. In addition, the maximum is at a much lower energy than for $K = 0.1$. Figure 9 shows the B_{2g} Raman susceptibility for the same parameters. This spectrum is similar to what we see for the parameters used in the main text. We do not show the A_{1g} susceptibility for these parameters

FIG. 9. The imaginary part of the Raman susceptibility for B_{2g} symmetry for $K = 0$, $J_2 = 0.57J_1$, and $J_3 = 0$. These parameters are found in the collinear stripe region near the transition to staggered dimer.
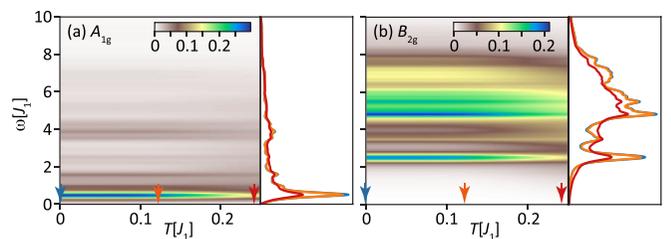
FIG. 11. The imaginary part of the Raman susceptibility for $K = 0.2J_1$, $J_2 = 0.47J_1$, and $J_3 = 0$ for A_{1g} (a) and B_{2g} (b) symmetries. These parameters are found in the collinear stripe region near the transition to staggered dimer.

since it is zero with the Raman operator we have used when $K = 0$.

Figure 10 shows the B_{1g} Raman susceptibility for $K = 0.2J_1$, again immediately inside the collinear stripe region. Here we see again a single peak that does not soften with increasing temperature. Figure 11 shows the A_{1g} and B_{2g}

susceptibilities. These are similar to the results shown in the main text with a single low energy peak in A_{1g} symmetry and a more spread out spectrum for B_{2g} symmetry. Again we see that the temperature dependence of the B_{1g} Raman susceptibility is what distinguishes the biquadratic coupling parameter used in the main text from other values.

[1] D. J. Scalapino, A common thread: The pairing interaction for unconventional superconductors, Rev. Mod. Phys. **84**, 1383 (2012).

[2] P. J. Hirschfeld, M. M. Korshunov, and I. I. Mazin, Gap symmetry and structure of Fe-based superconductors, Rep. Prog. Phys. **74**, 125508 (2011).

[3] J.-F. Ge, Z.-L. Liu, C. Liu, C.-L. Gao, D. Qian, Q.-K. Xue, Y. Liu, and J.-F. Jia, Superconductivity above 100 K in single-layer FeSe films on doped SrTiO₃, Nat. Mater. **14**, 285 (2015).

[4] Y. Mizuguchi, F. Tomioka, S. Tsuda, T. Yamaguchi, and Y. Takano, Superconductivity at 27 K in tetragonal FeSe under high pressure, Appl. Phys. Lett. **93**, 152505 (2008).

[5] S. Medvedev, T. M. McQueen, I. A. Troyan, T. Palasyuk, M. I. Eremets, R. J. Cava, S. Naghavi, F. Casper, V. Ksenofontov, G. Wortmann, and C. Felser, Electronic and magnetic phase diagram of β-Fe₁.₀₁Se with superconductivity at 36.7 K under pressure, Nat. Mater. **8**, 630 (2009).

[6] S. He, J. He, W. Zhang, L. Zhao, D. Liu, X. Liu, D. Mou, Y.-B. Ou, Q.-Y. Wang, Z. Li, L. Wang, Y. Peng, Y. Liu, C. Chen, L. Yu, G. Liu, X. Dong, J. Zhang, C. Chen, Z. Xu, X. Chen, X. Ma, Q. Xue, and X. J. Zhou, Phase diagram and electronic indication of high-temperature superconductivity at 65 K in single-layer FeSe films, Nat. Mater. **12**, 605 (2013).

[7] S. Tan, Y. Zhang, M. Xia, Z. Ye, F. Chen, X. Xie, R. Peng, D. Xu, Q. Fan, H. Xu, J. Jiang, T. Zhang, X. Lai, T. Xiang, J. Hu, B. Xie, and D. Feng, Interface-induced superconductivity and strain-dependent spin density waves in FeSe/SrTiO₃ thin films, Nat. Mater. **12**, 634 (2013).

[8] J. J. Lee, F. T. Schmitt, R. G. Moore, S. Johnston, Y.-T. Cui, W. Li, M. Yi, Z. K. Liu, M. Hashimoto, Y. Zhang, D. H. Lu, T. P. Devereaux, D.-H. Lee, and Z.-X. Shen, Interfacial mode coupling as the origin of the enhancement of T_c in FeSe films on SrTiO₃, Nature (London) **515**, 245 (2014).

[9] S. N. Rebec, T. Jia, C. Zhang, M. Hashimoto, D.-H. Lu, R. G. Moore, and Z.-X. Shen, Coexistence of Replica Bands and Superconductivity in FeSe Monolayer Films, Phys. Rev. Lett. **118**, 067002 (2017).

[10] F.-C. Hsu, J.-Y. Luo, K.-W. Yeh, T.-K. Chen, T.-W. Huang, P. M. Wu, Y.-C. Lee, Y.-L. Huang, Y.-Y. Chu, D.-C. Yan, and M.-K. Wu, Superconductivity in the PbO-type structure α-FeSe, Proc. Natl. Acad. Sci. USA **105**, 14262 (2008).

[11] Q. Si, R. Yu, and E. Abrahams, High-temperature superconductivity in iron pnictides and chalcogenides, Nat. Rev. Mater. **1**, 16017 (2016).

[12] T. M. McQueen, A. J. Williams, P. W. Stephens, J. Tao, Y. Zhu, V. Ksenofontov, F. Casper, C. Felser, and R. J. Cava, Tetragonal-to-Orthorhombic Structural Phase Transition at 90 K in the Superconductor Fe₁.₀₁Se, Phys. Rev. Lett. **103**, 057002 (2009).

[13] R. M. Fernandes, A. V. Chubukov, and J. Schmalian, What drives nematic order in iron-based superconductors? Nat. Phys. **10**, 97 (2014).

[14] M. G. Kim, R. M. Fernandes, A. Kreyssig, J. W. Kim, A. Thaler, S. L. Bud'ko, P. C. Canfield, R. J. McQueeney, J. Schmalian, and A. I. Goldman, Character of the structural and magnetic phase transitions in the parent and electron-doped BaFe₂As₂ compounds, Phys. Rev. B **83**, 134522 (2011).

[15] S. Avci, O. Chmaissem, D. Y. Chung, S. Rosenkranz, E. A. Goremychkin, J. P. Castellan, I. S. Todorov, J. A. Schlueter, H. Claus, A. Daoud-Aladine, D. D. Khalyavin, M. G. Kanatzidis, and R. Osborn, Phase diagram of Ba₁₋ₓKₓFe₂As₂, Phys. Rev. B **85**, 184507 (2012).

[16] C. R. Rotundu and R. J. Birgeneau, First- and second-order magnetic and structural transitions in BaFe₂₍₁₋ₓ₎Co₂ₓAs₂, Phys. Rev. B **84**, 092501 (2011).

[17] W. Bao, Y. Qiu, Q. Huang, M. A. Green, P. Zajdel, M. R. Fitzsimmons, M. Zhernenkov, S. Chang, M. Fang, B. Qian, E. K. Vehstedt, J. Yang, H. M. Pham, L. Spinu, and Z. Q. Mao, Tunable $(\delta\pi, \delta\pi)$-Type Antiferromagnetic Order in α-Fe(Te,Se) Superconductors, Phys. Rev. Lett. **102**, 247001 (2009).

[18] S. Li, C. de la Cruz, Q. Huang, Y. Chen, J. W. Lynn, J. Hu, Y.-L. Huang, F.-C. Hsu, K.-W. Yeh, M.-K. Wu, and P. Dai, First-order magnetic and structural phase transitions in Fe₁₊ᵧSeₓTe₁₋ₓ, Phys. Rev. B **79**, 054503 (2009).

[19] Q. Wang, Y. Shen, B. Pan, X. Zhang, K. Ikeuchi, K. Iida, A. D. Christianson, H. C. Walker, D. T. Adroja, M. Abdel-Hafiez, X. Chen, D. A. Chareev, A. N. Vasiliev, and J. Zhao, Magnetic ground state of FeSe, Nat. Commun. **7**, 12182 (2016).

[20] A. Chubukov, Pairing mechanism in Fe-based superconductors, Annu. Rev. Condens. Matter Phys. **3**, 57 (2012).

[21] J. K. Glasbrenner, I. I. Mazin, H. O. Jeschke, P. J. Hirschfeld, R. M. Fernandes, and R. Valentí, Effect of magnetic frustration on nematicity and superconductivity in iron chalcogenides, Nat. Phys. **11**, 953 (2015).

[22] A. Tamai, A. Y. Ganin, E. Rozbicki, J. Bacsa, W. Meevasana, P. D. C. King, M. Caffio, R. Schaub, S. Margadonna, K. Prassides, M. J. Rosseinsky, and F. Baumberger, Strong Electron Correlations in the Normal State of the Iron-Based FeSe₀.₄₂Te₀.₅₈ Superconductor Observed by Angle-Resolved Photoemission Spectroscopy, Phys. Rev. Lett. **104**, 097002 (2010).

[23] A. Yamasaki, Y. Matsui, S. Imada, K. Takase, H. Azuma, T. Muro, Y. Kato, A. Higashiya, A. Sekiyama, S. Suga, M. Yabashi, K. Tamasaku, T. Ishikawa, K. Terashima, H. Kobori, A. Sugimura, N. Umeyama, H. Sato, Y. Hara, N. Miyagawa, and S. I. Ikeda, Electron correlation in the FeSe superconductor studied by bulk-sensitive photoemission spectroscopy, Phys. Rev. B **82**, 184511 (2010).

[24] Z. P. Yin, K. Haule, and G. Kotliar, Kinetic frustration and the nature of the magnetic and paramagnetic states in iron pnictides and iron chalcogenides, Nat. Mater. **10**, 932 (2011).

[25] F. Wang, S. A. Kivelson, and D.-H. Lee, Nematicity and quantum paramagnetism in FeSe, Nat. Phys. **11**, 959 (2015).

[26] A. Baum, H. N. Ruiz, N. Lazarević, Y. Wang, T. Böhm, R. Hosseinian Ahangharnejhad, P. Adelmann, T. Wolf, Z. V. Popović, B. Moritz, T. P. Devereaux, and R. Hackl, Frustrated spin order and stripe fluctuations in FeSe, Commun. Phys. **2**, 14 (2019).

[27] I. Niesen and P. Corboz, A tensor network study of the complete ground state phase diagram of the spin-1 bilinear-biquadratic Heisenberg model on the square lattice, SciPost Phys. **3**, 030 (2017).

[28] N. Papanicolaou, Unusual phases in quantum spin-1 systems, Nucl. Phys. B **305**, 367 (1988).

[29] C. Yang, D. C. Sorensen, and R. B. Lehoucq, *ARPACK Users' Guide: Solution of Large-Scale Eigenvalue Problems with Implicitly Restarted Arnoldi Methods* (Siam, Philadelphia, 1998).

[30] E. Dagotto, Correlated electrons in high-temperature superconductors, Rev. Mod. Phys. **66**, 763 (1994).

[31] P. A. Fleury and R. Loudon, Scattering of light by one- and two-magnon excitations, Phys. Rev. **166**, 514 (1968).

[32] P. Massat, D. Farina, I. Paul, S. Karlsson, P. Strobel, P. Toulemonde, M.-A. Méasson, M. Cazayous, A. Sacuto, S. Kasahara, T. Shibauchi, Y. Matsuda, and Y. Gallais, Charge-induced nematicity in FeSe, Proc. Natl. Acad. Sci. USA **113**, 9177 (2016).

[33] C.-C. Chen, C. J. Jia, A. F. Kemper, R. R. P. Singh, and T. P. Devereaux, Theory of Two-Magnon Raman Scattering in Iron Pnictides and Chalcogenides, Phys. Rev. Lett. **106**, 067002 (2011).

[34] B. S. Shastry and B. I. Shraiman, Theory of Raman Scattering in Mott-Hubbard Systems, Phys. Rev. Lett. **65**, 1068 (1990).

[35] A. V. Chubukov and D. M. Frenkel, Resonant Two-Magnon Raman Scattering in Antiferromagnetic Insulators, Phys. Rev. Lett. **74**, 3057 (1995).

[36] A. V. Chubukov and D. M. Frenkel, Resonant two-magnon Raman scattering in parent compounds of high-T_c superconductors, Phys. Rev. B **52**, 9760 (1995).